Transfer-Free Synthesis of Atomically Precise Graphene Nanoribbons on Insulating Substrates

Zafer Mutlu[1,2], Juan Pablo Llinas[1,2], Peter H. Jacobse[3], Ilya Piskun[4], Raymond Blackwell[4], Michael F. Crommie[3,5,6], Felix R. Fischer[4,5,6], and Jeffrey Bokor[1,5,]*

[1]Department of Electrical Engineering and Computer Sciences, UC Berkeley, CA, 94720, U.S.A.

[2]The Molecular Foundry, Lawrence Berkeley National Laboratory, Berkeley, CA, 94720, U.S.A.

[3]Department of Physics, UC Berkeley, CA, 94720, U.S.A.

[4]Department of Chemistry, UC Berkeley, CA, 94720, U.S.A.

[5]Materials Sciences Division, Lawrence Berkeley National Laboratory, Berkeley, CA 94720, U.S.A.

[6]Kavli Energy NanoSciences Institute at the University of California Berkeley and the Lawrence Berkeley National Laboratory, Berkeley, CA 94720, U.S.A.

Corresponding author: Email: jbokor@berkeley.edu

The rational bottom-up synthesis of graphene nanoribbons (GNRs) provides atomically precise control of widths and edges that give rise to a wide range of electronic properties promising for electronic devices such as field-effect transistors (FETs). Since the bottom-up synthesis commonly takes place on catalytic metallic surfaces, the integration of GNRs into such devices

requires their transfer onto insulating substrates, which remains one of the bottlenecks in the development of GNR-based electronics. Herein, we report on a method for the transfer-free placement of GNRs on insulators. This involves growing GNRs on a gold film deposited onto an insulating layer followed by gentle wet etching of the gold, which leaves the nanoribbons to settle in place on the underlying insulating substrate. Scanning tunneling microscopy (STM) and Raman spectroscopy confirm that atomically precise GNRs of high density uniformly grow on the gold films deposited onto SiO_2/Si substrates and remain structurally intact after the etching process. We have also demonstrated transfer-free fabrication of ultra-short channel GNR FETs using this process. Our work here represents an important step towards large-scale integration of GNRs into electronic devices.

Keywords: graphene nanoribbons, bottom-up synthesis, FETs, STM, Raman spectroscopy

Graphene nanoribbons (GNRs) – nanometer-wide strips of single-atom-thick carbon sheet – are an exciting platform for studying diverse physical phenomena.[1,2] GNRs exhibit an electronic band gap that emerges from quantum confinement and edge effects[3] as well as localized electronic and quantum states associated with unique edge geometries[4,5] and can thus serve as key elements for post-silicon CMOS and quantum information devices. The width and edge structure of GNRs therefore need to be controlled with atomic precision to explore such functionalities and exploit them in potential applications. Recent advances in bottom-up synthesis have allowed production of atomically well-defined GNRs with different widths and edge topologies both in solution and on a substrate.[6,7] While the bulk-scale synthesis of long GNRs with a wide range of edge functionalities can be achieved in solution, cleanly and uniformly depositing such solution-synthesized GNRs on insulating substrates for high

performance electronic devices remains challenging. On the other hand, the on-surface synthesis allows the preparation of highly uniform, clean, and well separated GNRs with controlled coverage. The FETs with on-surface synthesized armchair GNRs exhibit high electrical performance.[8,9]

The integration of GNRs into FETs nevertheless requires physical transfer of GNRs onto insulating substrates since the common method for bottom-up synthesis of GNRs is catalyzed by the surface of coinage metals including gold, silver and copper, which are not compatible with transistor device operation.[10-12] Two main methods that are well-developed for the transfer of graphene have been adapted for the transfer of GNRs from metallic onto insulating substrates, wet-etch and electrochemical delamination.[13,14] The former is employed extensively in the transfer of GNRs grown on single crystalline gold thin films deposited onto insulator substrates, such as Au(111)/mica, wherein the gold is etched away after delamination of the gold/GNR film and transfer to a suitable device substrate.[15] On the other hand, the latter is used mostly in the transfer of GNRs grown on bulk gold single-crystal substrates, such as Au (788) and Au (111212), in which the gold growth substrate is preserved.[16,17] Nevertheless, both transfer procedures involve the physical transfer of mechanically delicate gold or polymer supported GNR films floating freely in aqueous solution onto a target substrate. GNRs can be folded, wrinkled, corrugated, and torn during this process, and the alignment between GNRs and the target substrate presents additional technical challenges.[18] Therefore, direct synthesis of GNRs on insulating substates without the transfer step is highly desirable but remains an unmet challenge.[19,20]

In this paper, we introduce a bottom-up method for transfer-free synthesis of GNRs on insulating substrates. The method incorporates growing GNRs on a thin gold layer deposited onto a target insulating substrate followed by gentle wet etching of the gold while leaving the GNRs intact on the substrate (Figure 1a). Seven atoms wide armchair GNRs (7-AGNRs) are examined in this work as a model GNR system because they are widely studied in the literature[6] and feature several well-defined characteristic Raman peaks that facilitate their characterization[21]. In principle this method should also work well for the synthesis of GNRs of various widths, such as 5-, 9- and 13-AGNRs.[22–24] We show that atomically precise 7-AGNRs of high density grow on the gold thin films deposited onto the SiO_2/Si substrates with sizes up to 2 × 2 inches without use of the single crystalline gold substates that are expensive and size-limited.[22,25] The GNRs settle intact on the substrate after etching of the gold. Furthermore, using our synthesis method, we successfully demonstrate transfer-free fabrication of short-channel 7-AGNR FETs.

RESULTS AND DISCUSSION

We first discuss the suitability of gold thin films that are deposited onto SiO_2/Si by e-beam evaporation under high-vacuum (HV) at 24 °C as growth substrates for atomically precise GNRs. Atomic force microscopy (AFM) and X-ray diffraction (XRD) are used for film characterization. Figure 1b,c shows the surface topography of a 100 nm thick gold thin film on a SiO_2/Si (Au/SiO_2/Si) substrate before and after annealing at 480 °C for 30 min in ultra-high vacuum (UHV), respectively. The as-deposited thin film has a granular morphology with a root mean square (rms) roughness of ~1.44 nm. Annealing substantially enhances the grain growth and lowers the surface roughness down to ~0.58 nm, which is comparable to that of the Au/mica substrates (Figure S1a) in which the gold is deposited under the same experimental conditions

and commercial Au(111)/mica substrates (Figure S1b) that have predominantly been used in previous GNR FET related studies.[26–30] We note that placing a two-dimensional (2D) hexagonal boron nitride (h-BN) flake on the SiO_2/Si substrate before the gold deposition can improve the surface and crystalline quality of the gold thin films (Figure S2).

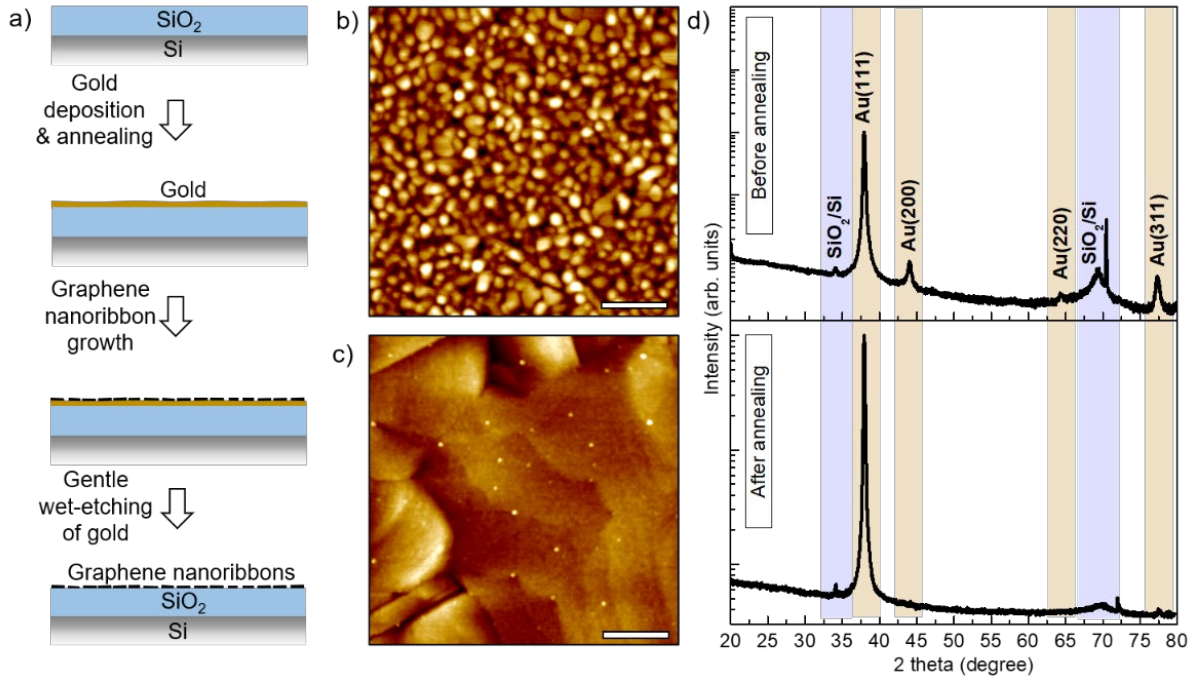

Figure 1. a) Schematic illustration of the transfer-free synthesis of GNRs on SiO_2/Si substrates. Typical AFM height images of a 100 nm gold thin film deposited onto a SiO_2/Si substrate b) before, and c) after annealing at 480 °C for 30 min in UHV. The scale bars are 200 nm. The rms surface roughness is measured to be ~1.44 nm and ~0.58 nm in b) and c), respectively. d) Corresponding XRD patterns of the Au/SiO_2/Si before and after annealing.

The crystallinity of the gold thin films on the SiO_2/Si before and after annealing is studied by XRD. As shown in Figure 1d, a typical XRD pattern of the Au/SiO_2/Si reveals a strong (111) peak and weak (200), (220) and (311) peaks as well as substrate-related peaks, indicating the

polycrystalline nature of the gold film.[31] After annealing, the (111) peak becomes the dominant feature while the other peaks disappear almost completely, suggesting that the gold film on the SiO_2/Si is mainly crystallized along the (111) direction,[31] similar to the Au/mica (Figure S1c) and commercial Au(111)/mica (Figure S1d). These results suggest that the Au/SiO_2/Si substrates are suitable for GNR growth.

Now, we discuss the growth and characterization of 7-AGNRs on the Au/SiO_2/Si substrates. 10,10′-dibromo-9,9′-bianthracene (DBBA) was deposited at high coverage (> 1 ML) onto the substrate held at 200 °C, leading to direct reaction of the monomers to form the polymer chains. This step was followed by high-temperature annealing at 400 °C to promote cyclodehydrogenation (CDH).[6] STM imaging (Figure 2a) of 7-AGNRs grown on the Au/mica substrate reveal densely packed GNRs covering the surface. Since the individual GNRs could not be resolved by STM due to the high density, we were not able to measure the exact length of the ribbons. However, the findings of previous studies using the similar growth recipe have shown that the lengths of 7-AGNRs can vary between subnanometer to several tens of nanometers.[6,9,32] The GNRs are randomly distributed on the surface of the gold films at large-scale but exhibit some degree of local alignment. In a previous study it has been shown that the straight surface steps of the Au(111) substrate promote the assembly of compact arrays of GNRs.[32] STM imaging also reveals the formation of quasi free-standing polymer chains atop the GNRs, which is commonly seen for high-density GNR growth.[33] Evidently, the hot-substrate growth process used here facilitates the formation of polymer adlayers, but these cannot be cyclized into GNRs since the bottom layer of polymers or GNRs intercalates the adlayer, effectively suppressing the catalytic activity of the gold that is necessary to achieve CDH.[34]

Raman spectroscopy is a fast and non-invasive analytical method that provides complementary valuable information about the GNR film at macroscopic scale. We thus characterized the GNRs by Raman spectroscopy using 532 nm wavelength laser excitation. This laser photon energy closely matches the E_{22} optical transition energy of 7-AGNRs,[35] resulting in strongly enhanced Raman intensity. Figure 2b shows a Raman spectrum of 7-AGNRs grown on the $Au/SiO_2/Si$ substrate. The most intense feature in the spectrum is the G-like mode at ~1601 cm^{-1} arising from C–C bond vibrations along the ribbon axis.[6] For 7-AGNRs, the shape, location and intensity of the G peak can vary by depending on the type or crystallinity of growth substrate, and doping.[35–37] The spectrum shows another well-defined peak at ~1343 cm^{-1}, labelled as D, which originates from a ring breathing mode of sp^2 atoms, resembling that of graphene.[38] Unlike graphene, for which the D band is activated only in the presence of defects, 7-AGNRs show a D peak even if they are defect-free, owing to their edges that are absent in pristine graphene. However, the linewidth and relative intensity of the D peak can still be used as a reliable probe for the structural quality of 7-AGNRs (Figure S3), along the lines of previous analyses of carbon nanotubes (CNTs) and graphene.[38,39] In this context, the presence of a sharp D peak with a low intensity relative to that of the G peak indicates a high degree of structural uniformity of 7-AGNRs.

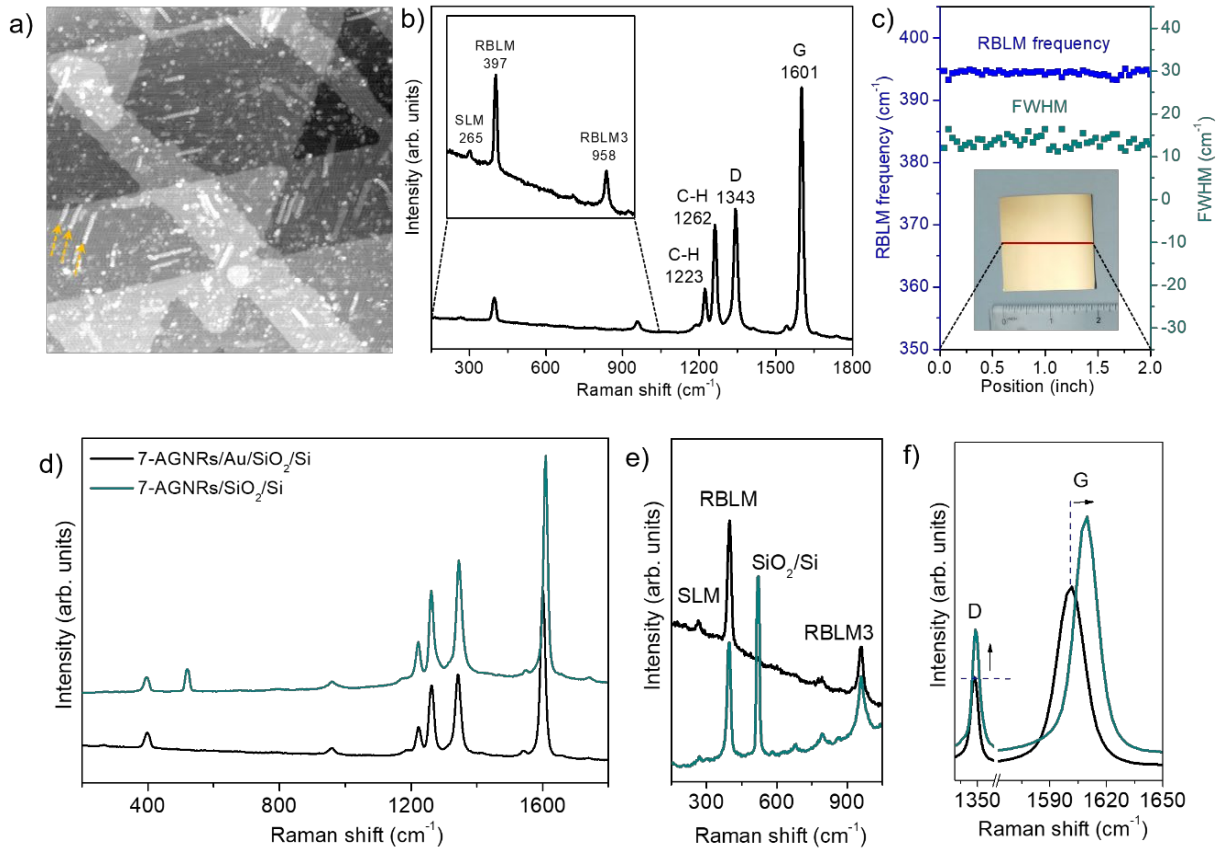

Figure 2. a) STM image (100 × 100 nm) of 7-AGNRs grown on the Au/mica. The arrows highlight the polymer chains on top of the GNRs. b) Typical Raman spectrum of 7-AGNRs grown on the Au/SiO_2/Si, collected with 532 nm excitation under ambient conditions. The inset shows the magnified view of the low-frequency region. c) The shift and FWHM of the RBLM peak measured from 50 different points on a 2 × 2 inch sample (shown in the inset). d) The Raman spectrum comparison of 7-AGNRs on the SiO_2/Si before and after etching of the gold. The comparison of the e) low-frequency region peaks and f) G peak of 7-AGNRs before and after etching of the gold.

In addition to the well-established G and D peaks, the Raman spectrum of 7-AGNRs contains several characteristic features owing to their nanoscale size. Near the D peak, the spectrum

reveals two additional peaks at ~1223 cm^{-1} and ~1262 cm^{-1}, which are associated with the theoretically predicted in-plane C–H bending modes localized along the edges.[40,41] The low-frequency region of the spectrum exhibits three distinct peaks. The peak at ~265 cm^{-1} corresponds to the shear-like mode (SLM).[42] The peaks at ~397 cm^{-1} and ~958 cm^{-1} are assigned to the radial-breathing like mode (RBLM)[42] and its third overtone, called RBLM3[42], respectively, in analogy to the radial-breathing mode (RBM) in CNTs[39]. The presence of the RBLMs can serve as a fingerprint of GNRs and their frequency provides valuable structural information.[43] Although the Raman spectrum is generated from a focal spot that covers more than tens of thousands of nanoribbons, the presence of only one sharp and intense RBLM peak confirms that virtually all GNRs are identical. To corroborate this point, the shift and FWHM of the RBLM mode – which has been shown to be highly sensitive for doping[44] and defects[45] – was measured at 50 different points on a 2 × 2 inch GNR sample, as shown in Figure 2c. The RBLM does not exhibit significant changes across the sample, indicating large-scale uniformity of 7-AGNRs.

We now demonstrate that 7-AGNRs grown on a gold thin film deposited onto a SiO_2/Si substrate naturally adhere to the underlying substrate after gentle wet etching of the gold with K/I_2, eliminating the need for the transfer. Unfortunately, imaging techniques, such as ambient AFM and scanning electron microscopy (SEM) are unable to resolve GNRs on SiO_2/Si due to GNR's extremely small dimensions, while STM is limited by the insulating nature of SiO_2/Si. Raman spectroscopy remains a powerful tool to confirm the presence of GNRs on SiO_2/Si,[15] and this technique was used to characterize the GNRs. Figure 2d shows the Raman spectrum of 7-AGNRs grown on the SiO_2/Si before and after etching of the gold. All GNR peaks are preserved without significant modification after etching, confirming that the GNRs remain structurally

intact.[15] In addition, the Raman spectrum of the GNRs on the SiO_2/Si obtained in our transfer-free method is virtually indistinguishable from that of a GNR sample prepared *via* the previously established transfer method (Figure S4a),[8] further confirming that both methods are viable in the synthesis of the GNRs on the SiO_2/Si. As can be seen in Figure 2e, no noticeable changes are observed in the width and position of the low-frequency characteristic Raman peaks of the GNRs, suggesting that no significant structural alteration occurs during etching.[15] On the other hand, after etching, the G peak is upshifted, and the intensity ratio of the D and G peaks is slightly increased (Figure 2f), which can be attributed to the interaction with the SiO_2/Si substrate.[35] Similar trends are observed in the Raman spectra of the transferred GNRs (Figure S4b).

Finally, we integrated 7-AGNRs into FET devices *via* both transfer-free and standard transfer methods to study their electrical transport properties. Figure 3a shows the schematic illustration of a 7-AGNR FET device fabricated in a local back gate geometry with a ~8 nm thick W gate capped with a ~5.5 nm HfO_2 gate dielectric (equivalent oxide thickness, EOT ≈ 1.5 nm), and Pd source-drain contacts. The local HfO_2 back gate has been proven to significantly improve the electrical performance of CNT transistors[46] as well as GNR transistors[8]. The GNRs were incorporated into the pre-patterned devices (Figure 3b) *via* both the standard transfer and transfer-free (the gold thin films were directly deposited onto the pre-patterned devices as shown in Figure S5) methods and then contacted with Pd source-drain contacts with a ~20 nm channel length by using electron beam lithography (EBL) (Figure 3c). Raman spectroscopy measurements (Figure S6) verify that the structural integrity of the GNRs is preserved after the etching and device fabrication process.[15]

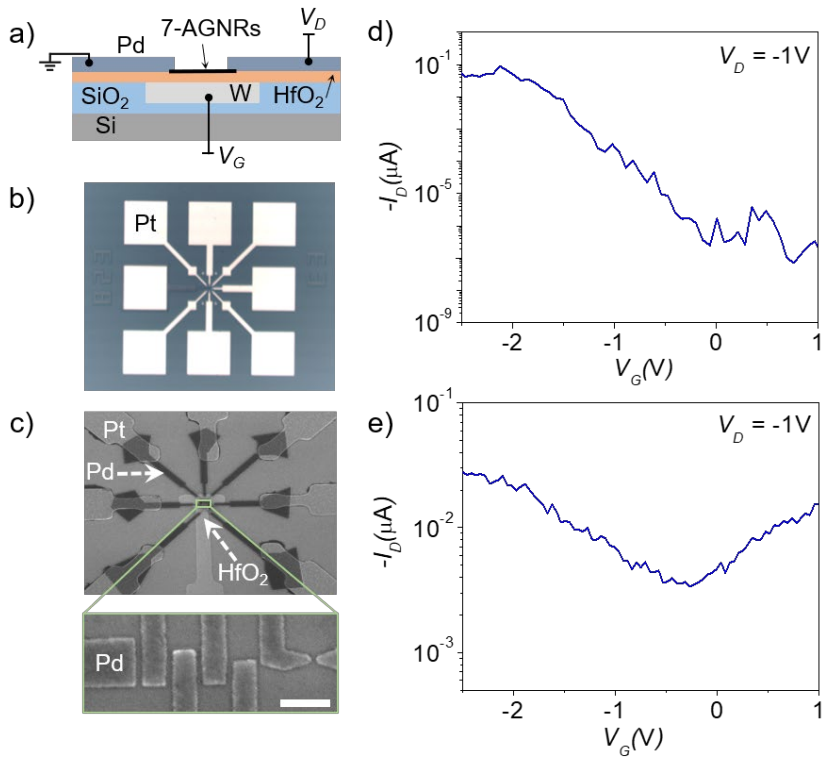

Figure 3. a) Schematic (not to scale) representation of 7-AGNR FETs with Pd source-drain electrodes and local HfO_2 back gate. b) Optical microscopy image of the FET arrays before the synthesis of the GNRs and patterning of the electrodes. c) SEM images of the devices after patterning of Pd electrodes. The scale bar is 200 nm. I_D-V_G characteristics of the FETs with the GNRs prepared with d) standard transfer and e) transfer-free methods.

Figure 3d displays drain-source current-gate voltage (I_D−V_G) behavior and a fixed drain-source voltage bias (V_D) of –1 V for a FET device made with the GNRs using the previous standard transfer process. The device exhibits excellent switching behavior with an on/off ratio of ~10^5 and on-state performance with an on-current (I_{on}) of ~60 nA, which are the highest to date among those of the FET devices made with 7-AGNRs,[9,16,26,47,48] confirming the high electrical quality of the GNRs grown on the gold thin films. We note that the blank FETs (GNR-free) do not show any conduction, and the gate leakage current of the GNR FETs is negligible compared to the

drain current (Figure S7a). The observed characteristics thus originate purely from the nanoribbons bridging the ~20 nm source-drain gap, not from the substrate or measurement artifacts. We ascribe this significant improvement of the electrical behavior to the enhanced gate efficiency achieved by adopting the local gate geometry with a thin high-κ HfO_2 gate dielectric[8] as well as to the increased number of the nanoribbons bridging to the source-drain gap due to the high surface coverage. We note that the GNR FETs exhibit a substantial device-to-device variation in the electrical performance (Figure S8). The variability could be arising from variations in contact length and number of GNRs in the channel that bridge the electrodes, line edge roughness in the electrode pattern, and sensitivity to oxide traps, etc.[8,46] Moreover, the devices exhibit a predominant *p*-type charge transport behavior, the origin of which is unclear at present and should be subjected to further investigations because it departs from the transport behavior of the 7-AGNR FETs in earlier reports.[9,16,47]

Figure 3g presents the I_D–V_G characteristic of a FET device with the GNRs obtained by the transfer-free method at a fixed V_D = –1 V. Similar to the transferred GNR FET device, it shows a particularly high I_{on} of ~ 30 nA. Nevertheless, the device operates as an ambipolar transistor exhibiting both electron and hole branches in the transfer characteristic and exhibits relatively higher gate leaking current (Figure S7b) and higher off-current resulting in a lower on/off ratio of ~10. Similar ambipolar transport behavior accompanied with low on/off ratio has also been observed in some 7-AGNR FET studies.[16,47] By further optimizing GNR growth and device fabrication process (see supplementary note and Figure S9), we expect to suppress the off-current in order to achieve high on/off ratio in the GNR FETs made *via* transfer-free process.

CONCLUSION

In conclusion, we demonstrate transfer-free synthesis of atomically precise GNRs on SiO_2/Si substrates as well as transfer-free fabrication of short channel GNR FETs. The structural integrity of the nanoribbons on the gold thin films is examined using Raman spectroscopy and STM characterization, while Raman measurements after etching of the gold verify that the GNRs remain intact on the SiO_2/Si substrate throughout. While gold is used in our method as a sacrificial metal catalyst for GNR growth, one could extend this technology to other metals such as copper. We thus anticipate that with additional synthesis and device optimization, high performance GNR FETs at large scale may become a reality.

EXPERIMENTAL SECTION

Materials Synthesis and Characterization

Gold substrate preparation: The gold thin films with a thickness of 100 nm were deposited onto SiO_2/Si (highly *p*-doped Si with a thermally grown 100 nm SiO_2) and freshly cleaved mica (SPI) substrates (unless otherwise specified) using an e-beam evaporator with deposition rate of ~0.1 nm s^{-1} and base pressure of ~1 × 10^{-6} Torr. Commercial Au(111)/mica substrate (Phasis, Switzerland) was also used for comparison purpose.

GNR growth: 7-AGNRs were grown from 10,10′-dibromo-9,9′-bianthracene (DBBA) monomers (Sigma-Aldrich) in a stand-alone industrial UHV system (Kurt J. Lesker) designed to allow for a fully automatized, reproducible and high-throughput (up to 6 inch in diameter) production. The growth recipe of 7-AGNRs can be described as follows: First, the gold substrates were manually

introduced into the lock chamber, which was then evacuated to a pressure of ~7×10^{-7} Torr, and were then transferred in the main chamber with a base pressure of ~1×10^{-9} Torr. Next, the surface of the gold substrates was treated with one sputtering/annealing cycle: 1 kV Ar^+ sputtering along the direction perpendicular to the substrates for ~5 min at 24 °C followed by annealing at 480 °C with a heating rate of 50 °C min^{-1} for 30 min. We note that annealing at 480 °C can lead to blister formation on the gold thin films deposited onto the SiO_2/Si substrates with sizes larger than 5 × 5 mm, which causes nonuniformity of the GNR coverage and thickness. Enhancing the surface adhesion of the substrate and lowering the process temperature can help overcome this problem. After that, DBBA was sublimed from an aluminum oxide crucible heated to 180 °C with a heating rate of 5 °C min^{-1} with the substrates held at 200 °C. After 5 min of deposition of DBBA, the samples were held at 200 °C for 20 min to activate the polymerization reaction, followed by annealing at 400 °C with a heating rate of 5 °C min^{-1} for 30 min to form 7-AGNRs *via* CDH.

Transfer-free method: The surface of the GNRs/Au/SiO_2/Si was covered with 2–3 drops of a potassium iodide (KI/I_2)-based gold etchant solution (Transene, GE-8148) to etch the gold layer. We note that thicker (>100 nm) gold thin films deposited onto bare SiO_2/Si substrates tend to quickly delaminate starting from the edges of the substrates as soon as placing etching solution due to low surface adhesion, which can result in nonuniformity of the GNR coverage and thickness. After ~5 min etching, the GNRs naturally settle on the substrates. The GNR/SiO_2/Si samples were then cleaned by soaking them in deionized water for 10 min followed by rinsing with isopropanol and finally dried under a stream of nitrogen.

Standard transfer method: The GNRs were transferred onto the SiO_2/Si substrates using standard transfer method[8] for comparison purpose. Standard transfer procedure can be described as follows: First, the GNRs grown on the Au/SiO_2/Si substrates were floated in 38% HCl in water, which caused the substrates to delaminate with the GNRs/Au film floating on the surface of the acid. Next, the floating GNRs/Au film was picked up with a SiO_2/Si substrate, with the GNRs facing the SiO_2 surface. At this stage, the gold films are usually not completely flat on the substrate. To increase adhesion between the gold films and substrates, a drop of isopropanol was placed onto the gold thin films and dried at ambient conditions until the gold films were fully flattened on the surface. The gold etching and subsequent cleaning procedure are the same as used in the transfer-free method.

AFM imaging: The surface topography of the samples was obtained by Bruker Dimension Icon AFM with ScanAsyst imaging and NanoScope software, operating in tapping mode at ambient conditions, using a Si probe (Bruker, RTESPA-300) with a tip radius of ~8 nm (force constant: ~40 N m^{-1}, resonance frequency: ~300 kHz). The height diagrams were recorded with scan sizes of 1 μm (unless otherwise specified) and scan speeds of 0.6 Hz (512 × 512 points). Nanoscope analysis software was used for AFM data analysis.

XRD characterization: The crystallinity of the gold films was studied by XRD measurements performed using a Siemens D5000 diffractometer operated in the θ°–2θ° mode, using Cu K_α radiation at 40 kV and 30 mA. The θ–2θ scans were collected in the 2θ range of 20°–80° with 0.01° step size and an acquisition time of 0.2 s *per* step.

Raman spectroscopy characterization: Raman characterization of the GNRs was performed using a Horiba Jobin Yvon LabRAM ARAMIS Raman microscope using 532 nm diode laser with <10 mW power each and a 100× objective lens, resulting in a laser spot size <1 μm. No thermal effects were observed under these measurement conditions, and at least three spectra from different points was collected for each sample.

STM imaging: After the growth of the GNRs on the Au/mica substrates, the samples were removed from the UHV chamber to air and inserted in another UHV system (Createc LT-STM) for STM characterization. To desorb contaminants accumulated during ambient exposure, first the samples were annealed at 350 °C for 30 min in the sample preparation chamber, after which they are transferred into the analysis chamber, with both chambers having a base pressure below 5×10^{-10} Torr. STM imaging was performed at liquid nitrogen temperature (T = –195.15 °C). Topographic STM images of the GNRs were recorded with 1.6 V sample bias and 30 pA setpoint current. Image processing of STM scans was done using WSxM software.[49]

Device Fabrication and Measurement

Preparation of HfO_2 local back gates: Pre-patterned local back-gate devices were used for the fabrication of the GNR FETs. Fabrication of the pre-patterned devices is described as follows: Using dry oxidation, 100 nm SiO_2 was grown on 150 mm Si wafers. The local back gates were lithographically patterned and dry etched into the SiO_2 followed by lift-off of a 8 nm W. ~5.5 nm HfO_2 was grown in an ALD system (Oxford, FlexAl Plasma ALD) at 135 °C. Alignment markers and large pads for electrical probing were patterned using standard photolithography and

lift-off of ~3 nm Cr and ~25 nm Pt. The wafer was then diced, and individual chips were used for further device processing.

GNR synthesis and patterning of source-drain electrodes: GNRs were integrated on the chips by both transfer-free (GNRs were grown on the gold thin films that are deposited onto the chips) and standard transfer methods, as described in materials synthesis and characterization section. After the GNR synthesis, *poly*-methyl methacrylate (molecular weight 950 kDa) was spun on the chips at 4,000 rpm and followed by a 10 min bake at 180 °C. Next, the source-drain electrodes (~20–200 nm wide, ~20 nm gaps) were patterned using a JEOL 6300-FS 100 kV EBL system and subsequently developed in 3:1 IPA: MIBK at 5 °C for 90 s. Finally, 12 nm Pd was deposited using e-beam evaporation (Kurt J. Lesker) and lift-off was completed in Remover PG at 80 °C.

Electrical characterization: The electrical characterization of the GNR FETs was performed in the Lakeshore CPX-HF probe with the Agilent 4155C semiconductor parameter analyzer and EasyEXPERT software at ambient conditions.

ASSOCIATED CONTENT

Supporting Information

The Supporting Information is available free of charge *via* the Internet at http://pubs.acs.org. Additional optical microscopy, AFM, XRD, and Raman spectroscopy and transport measurement results.

Author Contributions

The manuscript was written through contributions of all authors. All authors have given approval to the final version of the manuscript.

ACKNOWLEDGMENT

This work was supported in part by the Office of Naval Research (ONR) MURI Program N00014-16-1-2921 and the NSF Center for Energy Efficient Electronics Science. Raman spectroscopy characterization, charge transport measurements and atomic layer deposition were performed at the Molecular Foundry at Lawrence Berkeley National Laboratory (LBNL), supported by the Office of Science, Office of Basic Energy Sciences, of the U.S. Department of Energy (DOE) under contract No. DE-AC02-05CH11231. Device fabrication was performed at the Stanford Nano Shared Facilities (SNSF) at Stanford University, supported by the National Science Foundation (NSF) under award ECCS-1542152. P.H.J. acknowledges funding from the Dutch Research Council through Rubicon award 019.182EN.018. Part of this work was also performed at the Marvell Nanofabrication Laboratory at the University of California Berkeley. We thank N. Gupta and A. Javey for access to atomic force microscopy and E. Chan for access to Raman spectroscopy.

References

[1] Smith, S.; Llinás, J. -P.; Bokor, J.; Salahuddin, S. Negative Differential Resistance and Steep Switching in Chevron Graphene Nanoribbon Field-Effect Transistors. *IEEE Electron Device Lett*. **2017**, 39, 143−146.

[2] Cao, T.; Zhao, F.; Steven, G. L. Topological Phases in Graphene Nanoribbons: Junction States, Spin Centers, and Quantum Spin Chains. *Phys. Rev. Lett.* **2017**, 119, 076401.

[3] Son, Y-W.; Cohen, M. L.; Louie, S. G. Energy Gaps in Graphene Nanoribbons. *Phys. Rev. Lett.* **2006**, 97, 216803.

[4] Rizzo, D. J.; Veber, G.; Cao, T.; Bronner, C.; Chen, T.; Zhao, F.; Rodriguez, H.; Louie, S. G.; Crommie, M. F.; Fischer, F. R. Topological Band Engineering of Graphene Nanoribbons. *Nature* **2018**, 560, 204−208.

[5] Gröning, O.; Wang, S.; Yao, X.; Pignedoli, C. A.; Barin, G. B.; Daniels, C.; Cupo, A.; Meunier, V.; Feng, X.; Narita, A.; Müllen, K. Engineering of Robust Topological Quantum Phases in Graphene Nanoribbons. *Nature* **2018**, 560, 209−213.

[6] Cai, J.; Ruffieux, P.; Jaafar, R.; Bieri, M.; Braun, T.; Blankenburg, S.; Muoth, M.; Seitsonen, A.P.; Saleh, M.; Feng, X.; Müllen, K. Atomically Precise Bottom-Up Fabrication of Graphene Nanoribbons. *Nature* **2010**, 466, 470−473.

[7] Vo, T. H.; Shekhirev, M.; Kunkel, D. A.; Morton, M. D.; Berglund, E.; Kong, L.; Wilson, P. M.; Dowben, P. A.; Enders, A.; Sinitskii, A. Large-Scale Solution Synthesis of Narrow Graphene Nanoribbons. *Nat. Commun* **2014**, 5, 3189.

[8] Llinas, J. P.; Fairbrother, A.; Barin, G. B.; Shi, W.; Lee, K.; Wu, S.; Choi, B.Y.; Braganza, R.; Lear, J.; Kau, N.; Choi, W. Short-Channel Field-Effect Transistors with 9-Atom and 13-Atom Wide Graphene Nanoribbons. *Nat. Commun* **2017**, 8, 633.

[9] Bennett, P. B.; Pedramrazi, Z.; Madani, A.; Chen, Y. C.; de Oteyza, D. G.; Chen, C.; Fischer, F. R.; Crommie, M. F; Bokor, J. Bottom-up Graphene Nanoribbon Field-Effect Transistors. *Appl. Phys. Lett.* **2013**, 103, 253114.

[10] Jacobse, P. H.; Kimouche, A.; Gebraad, T.; Ervasti, M. M.; Thijssen, J. M.; Liljeroth, P.; Swart, I. Electronic Components Embedded in A Single Graphene Nanoribbon. *Nat. Commun.* **2017**, 8, 1−7.

[11] Jacobse, P. H.; Simonov, K. A.; Mangnus, M. J.; Svirskiy, G. I.; Generalov, A. V.; Vinogradov, A. S.; Sandell, A.; Mårtensson, N.; Preobrajenski, A. B.; Swart, I. One Precursor but Two Types of Graphene Nanoribbons: On-Surface Transformations of 10, 10′-Dichloro-9, 9′-bianthryl on Ag (111). *J. Phys. Chem. C* **2019**, 123, 8892−8901.

[12] Schulz, F.; Jacobse, P. H.; Canova, F. F.; Van Der Lit, J.; Gao, D. Z.; Van Den Hoogenband, A.; Han, P.; Klein Gebbink, R. J.; Moret, M. E.; Joensuu, P. M.; Swart, I. Precursor Geometry Determines the Growth Mechanism in Graphene Nanoribbons. *J. Phys. Chem. C* **2017**, 121, 2896−2904.

[13] Kim, K. S.; Zhao, Y.; Jang, H.; Lee, S. Y.; Kim, J. M.; Kim, K. S.; Ahn, J. H.; Kim, P.; Choi, J. Y.; Hong, B. H. Large-Scale Pattern Growth of Graphene Films For Stretchable Transparent Electrodes. *Nature* **2009**, 457, 706−710.

[14] Wang, Y.; Zheng, Y.; Xu, X.; Dubuisson E.; Bao. Q.; Lu J.; Loh K. P. Electrochemical Delamination of CVD-Grown Graphene Film: Toward the Recyclable Use of Copper Catalyst. *ACS Nano* **2011**, 5, 9927.

[15] Borin B. G.; Fairbrother, A.; Rotach, L.; Bayle, M.; Paillet, M.; Liang, L.; Meunier, V.; Hauert, R.; Dumslaff, T.; Narita, A.; Müllen, K. Surface-Synthesized Graphene Nanoribbons for

Room Temperature Switching Devices: Substrate Transfer and *Ex Situ* Characterization. *ACS Appl. Nano Mater.* **2019**, 2, 2184−2192.

[16] Passi, V.; Gahoi, A.; Senkovskiy, B. V.; Haberer, D.; Fischer, F. R.; Grüneis, A.; Lemme, M. C. Field-Effect Transistors Based on Networks of Highly Aligned, Chemically Synthesized N=7 Armchair Graphene Nanoribbons. *ACS Appl. Mater. Interfaces* **2018**, 10, 9900−9903.

[17] Zhao, S.; Barin, G. B.; Cao, T.; Overbeck, J.; Darawish, R.; Lyu, T.; Drapcho, S.; Wang, S.; Dumslaff, T.; Narita, A.; Calame, M. Optical Imaging and Spectroscopy of Atomically Precise Armchair Graphene Nanoribbons. *Nano Lett.* **2020**, 20, 1124−1130.

[18] Kang, J.; Shin, D.; Bae, S.; Hong, B. H. Graphene Transfer: Key for Applications. *Nanoscale* **2012**, 4, 5527−5537.

[19] Kolmer, M.; Ahmad Zebari, A. A.; Prauzner-Bechcicki, J. S.; Piskorz, W.; Zasada, F.; Godlewski, S.; Such, B.; Sojka, Z.; Szymonski, M. Polymerization of Polyanthrylene on A Titanium Dioxide (011)-(2×1) Surface. *Angew. Chem* **2013**, 52, 10300−10303.

[20] Kolmer, M.; Steiner, A. K.; Izydorczyk, I.; Ko, W.; Engelund, M.; Szymonski, M.; Li, A. P.; Amsharov, K. Rational Synthesis of Atomically Precise Graphene Nanoribbons Directly on Metal Oxide Surfaces. *Science* **2020**, 369, 571−575.

[21] Overbeck, J.; Barin, G. B.; Daniels, C.; Perrin, M.L.; Liang, L.; Braun, O.; Darawish, R.; Burkhardt, B.; Dumslaff, T.; Wang, X. Y.; Narita, A. Optimized Substrates and Measurement Approaches for Raman Spectroscopy of Graphene Nanoribbons. *Phys. Status Solidi B* **2019**, 256, 1900343.

[22] El Abbassi, M.; Perrin, M. L.; Barin, G. B.; Sangtarash, S.; Overbeck, J.; Braun, O.; Lambert, C. J.; Sun, Q.; Prechtl, T.; Narita, A.; Müllen, K. Controlled Quantum Dot Formation

in Atomically Engineered Graphene Nanoribbon Field-Effect Transistors. *ACS Nano* **2020**, 14, 5754−5762.

[23] Talirz, L.; Söde, H.; Dumslaff, T.; Wang, S.; Sanchez-Valencia, J. R.; Liu, J.; Shinde, P.; Pignedoli, C. A.; Liang, L.; Meunier, V.; Plumb, N. C. On-Surface Synthesis and Characterization of 9-Atom Wide Armchair Graphene Nanoribbons. *ACS Nano* **2017**, 11, 1380−1388.

[24] Chen, Y. C.; De Oteyza, D. G.; Pedramrazi, Z.; Chen, C.; Fischer, F. R.; Crommie, M. F. Tuning the Band Gap of Graphene Nanoribbons Synthesized from Molecular Precursors. *ACS Nano* **2013**, 7, 6123−6128.

[25] Sun, Q.; Gröning, O.; Overbeck, J.; Braun, O.; Perrin, M. L.; Borin Barin, G.; El Abbassi, M.; Eimre, K.; Ditler, E.; Daniels, C.; Meunier, V. Massive Dirac Fermion Behavior in a Low Bandgap Graphene Nanoribbon Near a Topological Phase Boundary. *Adv. Mater.* **2020**, 32, 1906054.

[26] Fairbrother, A.; Sanchez-Valencia, J. R.; Lauber, B.; Shorubalko, I.; Ruffieux, P.; Hintermann, T.; Fasel, R. High Vacuum Synthesis and Ambient Stability of Bottom-Up Graphene Nanoribbons. *Nanoscale* **2017**, 9, 2785−2792.

[27] Candini, A.; Martini, L.; Chen, Z.; Mishra, N.; Convertino, D.; Coletti, C.; Narita, A.; Feng, X.; Müllen, K.; Affronte, M. High Photoresponsivity in Graphene Nanoribbon Field-Effect Transistor Devices Contacted with Graphene Electrodes. *J. Phys. Chem. C* **2017**, 121, 10620−10625.

[28] Richter, N.; Chen, Z.; Tries, A.; Prechtl, T.; Narita, A.; Müllen, K.; Asadi, K.; Bonn, M.; Kläui, M. Charge Transport Mechanism in Networks of Armchair Graphene Nanoribbons. *Sci. Rep.* **2020**, 10, 1988.

[29] Martini, L.; Chen, Z.; Mishra, N.; Barin, G. B.; Fantuzzi, P.; Ruffieux, P.; Fasel, R.; Feng, X.; Narita, A.; Coletti, C.; Müllen, K. Structure-Dependent Electrical Properties of Graphene Nanoribbon Devices with Graphene Electrodes. *Carbon* **2019**, 146, 36−43.

[30] Sakaguchi, H.; Song, S.; Kojima, T.; Nakae, T. Homochiral Polymerization-Driven Selective Growth of Graphene Nanoribbons. *Nat. Chem.* **2017**, 9, 57.

[31] Uosaki, K.; Shen, Y.; Kondo, T. Preparation of A Highly Ordered Au (111) Phase on A Polycrystalline Gold Substrate by Vacuum Deposition and Its Characterization by XRD, GISXRD, STM/AFM, and Electrochemical Measurements. *J. Phys. Chem* **1995**, 99, 14117−14122.

[32] Ma, C.; Xiao, Z.; Lu, W.; Huang, J.; Hong, K.; Bernholc, J.; Li, A. P. Step Edge-Mediated Assembly of Periodic Arrays of Long Graphene Nanoribbons on Au (111). *Chem. Commun.* **2019**, 55, 11848−11851.

[33] Ma, C.; Xiao, Z.; Zhang, H.; Liang, L.; Huang, J.; Lu, W.; Sumpter, B. G.; Hong, K.; Bernholc, J.; Li, A.P. Controllable Conversion of Quasi-Freestanding Polymer Chains to Graphene Nanoribbons. *Nat. Commun* **2017**, 8, 14815.

[34] Xiao, Z.; Ma, C.; Lu, W.; Huang, J.; Liang, L.; Hong, K.; Li, A. P., Sumpter, B. G., Bernholc, J. *Ab Initio* Investigation of The Cyclodehydrogenation Process for Polyanthrylene Transformation to Graphene Nanoribbons. *Npj Comput. Mater.* **2019**, 5, 91.

[35] Senkovskiy, B. V.; Pfeiffer, M.; Alavi, S. K.; Bliesener, A.; Zhu, J.; Michel, S.; Fedorov, A. V.; German, R.; Hertel, D.; Haberer, D.; Petaccia, L. Making Graphene Nanoribbons Photoluminescent. *Nano Lett.* **2017**, 17, 4029−4037.

[36] Huang, H.; Wei, D.; Sun, J.; Wong, S. L.; Feng, Y. P.; Neto, A. C.; Wee, A. T. S. Spatially Resolved Electronic Structures of Atomically Precise Armchair Graphene Nanoribbons. *Sci. Rep.* **2012**, 2, 983.

[37] Senkovskiy, B. V.; Fedorov, A. V.; Haberer, D.; Farjam, M.; Simonov, K. A.; Preobrajenski, A. B.; Mårtensson, N.; Atodiresei, N.; Caciuc, V.; Blügel, S.; Rosch, A. Semiconductor-to-Metal Transition and Quasiparticle Renormalization in Doped Graphene Nanoribbons. *Adv. Electron. Mater.* **2017**, 3, 1600490.

[38] Ferrari, A. C.; Basko, D. M. Raman Spectroscopy as A Versatile Tool for Studying the Properties of Graphene. *Nat. Nanotechnol* **2013**, 8, 235−246.

[39] Dresselhaus, M. S.; Dresselhaus, G.; Saito, R.; Jorio, A. Raman Spectroscopy of Carbon Nanotubes. *Phys. Rep.* **2005**, 409, 47−99.

[40] Yamada, M., Yamakita, Y., Ohno, K., Phonon Dispersions of Hydrogenated and Dehydrogenated Carbon Nanoribbons. *Phys. Rev. B* **2008**, 77, 054302.

[41] Gillen, R.; Mohr, M.; Thomsen, C.; Maultzsch, J. Vibrational Properties of Graphene Nanoribbons by First-Principles Calculations. *Phys. Rev. B* **2009**, 80, 155418.

[42] Ma, C.; Liang, L.; Xiao, Z.; Puretzky, A. A.; Hong, K.; Lu, W.; Meunier, V.; Bernholc, J.; Li, A. P. Seamless Staircase Electrical Contact to Semiconducting Graphene Nanoribbons. *Nano Lett.* **2017**, 17, 6241−6247.

[43] Zhou, J.; Dong, J. Vibrational Property, and Raman Spectrum of Carbon Nanoribbon. *Appl. Phys. Lett* **2007**, 91, 173108.

[44] Senkovskiy, B. V.; Usachov, D. Y.; Fedorov, A. V.; Marangoni, T.; Haberer, D.; Tresca, C.; Profeta, G.; Caciuc, V.; Tsukamoto, S.; Atodiresei, N.; Ehlen, N. Boron-Doped Graphene Nanoribbons: Electronic Structure and Raman Fingerprint. *ACS Nano* **2018**, 12, 7571−7582.

[45] Ma, C.; Xiao, Z.; Puretzky, A. A.; Baddorf, A. P.; Lu, W.; Hong, K.; Bernholc, J.; Li, A. P.; Oxidization Stability of Atomically Precise Graphene Nanoribbons. *Phys. Rev. Materials* **2018**, 2, 014006.

[46] Pitner, G.; Hills, G.; Llinas, J. P.; Persson, K. M.; Park, R.; Bokor, J.; Mitra, S.; Wong, H. S. P. Low-Temperature Side Contact to Carbon Nanotube Transistors: Resistance Distributions Down to 10 nm Contact Length. *Nano Lett.*, **2019**, 19, 1083−1089.

[47] Ohtomo, M.; Sekine, Y.; Hibino, H.; Yamamoto, H. Graphene Nanoribbon Field-Effect Transistors Fabricated by Etchant-Free Transfer from Au (788). *Appl. Phys. Lett.* **2018**, 112, 021602.

[48] Horcas, I.; Fernández, R.; Gomez-Rodriguez, J. M.; Colchero, J. W. S. X.; Gómez-Herrero, Baro, A. M. WSXM: A Software for Scanning Probe Microscopy and A Tool for Nanotechnology, *Rev Sci Instrum* **2007**, 78, 013705.

ToC figure: